ACS APPLIED BIO MATERIALS

www.acsabm.org Article

Extracellular Ca^{2+}-Sensing Fluorescent Protein Biosensor Based on a Collagen-Binding Domain

Irina A. Okkelman, Ryan McGarrigle, Shane O'Carroll, Daniel Carvajal Berrio, Katja Schenke-Layland, James Hynes, and Ruslan I. Dmitriev*

Cite This: *ACS Appl. Bio Mater.* 2020, 3, 5310−5321 Read Online

ACCESS | Metrics & More | Article Recommendations | Supporting Information

ABSTRACT: The importance of extracellular gradients of biomolecules is increasingly appreciated in the processes of tissue development and regeneration, in health and disease. In particular, the dynamics of extracellular calcium concentration is rarely studied. Here, we present a low affinity Ca^{2+} biosensor based on Twitch-2B fluorescent protein fused with the cellulose- and collagen-binding peptides. These recombinant chimeric proteins can bind cellulose and collagen scaffolds and enable scaffold-based biosensing of Ca^{2+} in the proximity of cells in live 3D tissue models. We found that the Twitch-2B mutant is compatible with intensity-based ratiometric and fluorescence lifetime imaging microscopy (FLIM) measurement formats, under one- and two-photon excitation modes. Furthermore, the donor fluorescence lifetime of the biosensor displays response to $[Ca^{2+}]$ over a range of ∼2−2.5 ns, making it attractive for multiplexed FLIM assays. To evaluate the performance of this biosensor in physiological measurements, we applied it to the live Lgr5-GFP mouse intestinal organoid culture and measured its responses to the changes in extracellular Ca^{2+} upon chelation with EGTA. When combined with spectrally resolved FLIM of lipid droplets using Nile red dye, we observed changes in cytoplasmic and basal membrane-associated lipid droplet composition in response to the extracellular Ca^{2+} depletion, suggesting that the intestinal epithelium can respond to and compensate such treatment. Altogether, our results demonstrate Twitch-2B as a prospective Ca^{2+} sensor for multiplexed FLIM analysis in a complex 3D tissue environment.

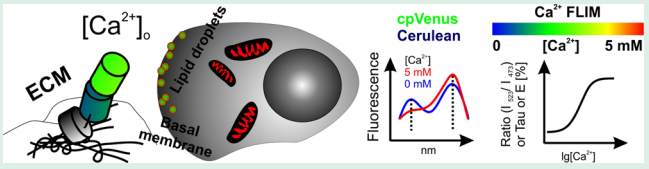

KEYWORDS: *biosensor, calcium, extracellular matrix, fluorescence lifetime imaging microscopy (FLIM), intestinal organoids*

INTRODUCTION

Extracellular cues become increasingly important in understanding of tissue organization and development. Successful tissue assembly from stem cell-derived organoids depends on the time-dependent changes of various biophysical parameters experienced during growth and differentiation.[1] In addition to physical tension[2] and the extracellular matrix itself,[3] changing cell density and composition can also affect gradients of O_2 (hypoxia),[4] distribution and diffusion of reactive oxygen species, peptides and growth factors, pH, and other ions such as Ca^{2+}.[5]

A number of reports have indicated the role of extracellular Ca^{2+} as one of the primary signals that influence the cell function;[6] thus, regulation of extracellular Ca^{2+} has shown to be relevant to gastrointestinal tract function,[7] bone marrow,[8] brain and CNS function,[9] smooth and skeletal muscles,[10] wound healing,[11] plasma membrane repair,[12] engineered organoid-like tissues,[13] and microbial biofilm formation.[14] Every mammalian cell relies on Ca^{2+} homeostasis, which in turn is tightly regulated through the activities of ion channels and ATPases, Na^+/Ca^{2+} exchangers, cytosolic Ca^{2+}-binding proteins, and various depots such as endoplasmic reticulum, secretory vesicles, and mitochondria.[15−17] Calcium influx and efflux processes through the plasma membrane are tightly regulated, and the ability to sense peri- and extracellular Ca^{2+} dynamics can become a valuable tool for probing cell function without the need of labeling it.

However, Ca^{2+} sensors with affinity in the range of 0−10 mM are rarely realized in optical imaging and analytical measurements.[18−20] The main challenges in sensing extracellular Ca^{2+} ($[Ca^{2+}]_o$) with most of the experimental *in vitro* cell-based models are (i) relatively large extracellular volume surrounding the cells, resulting in a quick equilibrium of Ca^{2+} across the whole volume and (ii) the lack of suitable fluorescent probes and protein biosensors.[6,21]

Biosensor scaffold materials based on the labeling of solid and gel-based materials can be employed in cell and tissue engineering and provide additional chemo-/biosensing functionalities.[4,22−33] The sensing molecule is deposited at or attached to the fiber or the scaffold material and not diffusely distributed across the sample; in some cases, this approach is

Received: May 29, 2020
Accepted: July 17, 2020
Published: July 17, 2020

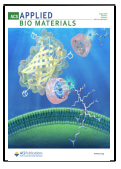

https://dx.doi.org/10.1021/acsabm.0c00649
ACS Appl. Bio Mater. 2020, 3, 5310−5321

very similar to the use of O_2-sensing films and foils.[34−37] Materials employed in the production of scaffolds for tissue engineering can be either synthetic (*e.g.* polymer-based) or bio- and macromolecule-based materials, for example, produced from natural hydrogels, decellularized (DC) materials, and other moieties. Thus, different approaches are needed for the deposition of sensing molecules, and these can be achieved *via* physical impregnation, covalent conjugation, or through specific biomolecular interactions. Physical entrapment of hydrophobic dyes can be provided by electrospinning and solvent-swelling methods.[4,24,26] Covalent immobilization was reported for many organic polymers including fluorescent pH-sensing proteins.[38,39] Recently, specific biorecognition-based binding was described for producing biosensor cellulose materials, with the help of cellulose-binding domain (CBD).[25] In this approach, biocompatible scaffolds and biosensor proteins are used, making them an attractive option for advanced biosensor design.

A vast number of Förster resonance energy transfer (FRET)-based protein "GECI" biosensors of various structures and origins enable sensing of Ca^{2+}.[20,40−42] Traditionally, sensing of Ca^{2+} was focused on the temporal resolution of Ca^{2+} fluxes and not on measuring their magnitude. Troponin-based FRET Ca^{2+}-sensing biosensors such as Twitch-2B are highly attractive for quantitative ratiometric and potentially fluorescence lifetime imaging microscopy (FLIM)-based measurements.[43−45] The latter approach, often relying on measurement of the fluorescence lifetime or FRET efficiency of the donor fluorescent protein, is promising for quantitative *in vitro* and *in vivo* measurements: it is less susceptible to the differences in tissue light absorption and scattering (which can represent a problem with detecting two different emission wavelengths), often enables absolute calibration, and is compatible with two-photon excited deep tissue imaging.[43,45,46]

Griesbeck and co-workers reported a number of "Twitch" biosensors with tunable affinity and improved performance for ratiometric sensing, with one mutant (Twitch-2B 54S+) showing promising analytical properties for extracellular measurements.[44] Here, we further evaluated its use for the production of cellulose- and collagen-based extracellular Ca^{2+}-sensing scaffold materials and found attractive features for biosensing in ratiometric and FLIM detection modalities, enabling multiparameter imaging of 3D tissue models such as stem cell-derived intestinal organoids.

EXPERIMENTAL SECTION

Antarctic phosphatase and restriction enzymes were purchased from New England Biolabs (Brennan & Co, Dublin, Ireland). T4 DNA Ligase, polymerase chain reaction (PCR) buffer, and Wizard Mini-Preps Plasmid DNA purification and SV Gel Clean-up kits were purchased from Promega (MyBio, Ireland). The O_2-sensitive phosphorescent probe Pt-Glc was synthesized as described previously.[47] DC celery scaffolds were prepared essentially as described previously.[25]

Tetramethylrhodamine methyl ester (TMRM), Nile red, CelLytic B reagent, protease inhibitors, lysozyme, Bradford protein assay reagent, LB Broth, and all the other reagents were from Sigma-Aldrich (Dublin, Ireland).

Standard sterile TC plates and plastic were from Sarstedt (Germany); collagen I-coated plates and half-area plates were from Greiner (Cruinn, Dublin, Ireland). Microfluidic channel slides μ-Slide VI$^{0.1}$ and multiwell silicone inserts were from Ibidi GmbH (Martinsried, Germany).

Molecular Cloning and Production of Recombinant Proteins. Plasmid DNA encoding Twitch-2B 54S+ low affinity mutant generously provided by Prof. O. Griesbeck was prepared as described previously.[44] An insert encoding the ORF was PCR-amplified using primers 5′-GATCGG-TACCGGTGGTGGTTCTGGTGGTATGGTGAGCAAGGGC-GAGG-3′ (forward) and 5′-AGTCGGTACCTCAATCCT-CAATGTTGTGACGGA-3′ (reverse) and cloned using the *Kpn*I site into the CBD Δ(FTN) vector essentially as described before,[25] in order to produce the CBD-Twitch expression construct.

For collagen-binding domain (ColBD)-Twitch, we used a custom-synthesized (Genscript, USA) sequence encoding N-terminal 6xHis tag, von Willebrand Factor (vWF) peptide WREPSFMALS, and Twitch-2B 54S+ (cloned using *Kpn*I site). All the produced expression constructs were verified using sequencing (GATC Biotech AG). Expression constructs were propagated in *Escherichia coli* SG13009 cells, expressed (0.125 mM IPTG, room temperature, 18 h for ColBD-Twitch and 0.25 mM IPTG, 4 °C, 72 h for CBD-Twitch), and purified essentially as described previously with the CBD-ECFP protein.[25] Purified proteins were dialyzed against PBS and stored at 4 °C. The total protein concentration was assessed using Bradford assay (Sigma) and spectrophotometrically (considering ε_{515} = 83,000 M^{-1} cm^{-1} for Ca^{2+}-free form of cpVenus). Typical protein yields were 7 mg/L (CBD-Twitch, 49−80% folding rate) and >60 mg/L (ColBD-Twitch, 55−70% folding rate).

Scaffolds and Coatings. Various types of collagen-based matrices were used in the study: 96-well flat bottom plates or DC celery coated with collagen IV from the human placenta diluted as described in ref 48, black-walled collagen I precoated 96-well plates (Greiner 655956), and Matrigel ("growth factor reduced" grade, Corning, 356231) was either distributed as the monolayer (15 μL per well of half-area plates, Greiner 675161) or drop-casted on 35 mm microscopy imaging dishes. Proteins (CBD-Twitch or ColBD-Twitch) were diluted in phosphate-buffered saline (PBS, pH 7.4), 0.135 M NaCl, or organoid growth media, added to the collagen or Matrigel matrices, and incubated for 0.5−16 h at room temperature before analysis.

Mouse Intestinal Organoid Culture. Mouse Lgr5-GFP organoids were cultured as described previously.[49] To stain Matrigel, ColBD-Twitch was added to the organoid culture in a complete growth medium (1 μM, 1 h), washed once, and imaged in Phenol red-free DMEM medium (Sigma-Aldrich, D5030) supplemented with 10 mM HEPES, pH 7.2, 10 mM D-glucose, 2 mM L-glutamine, and 1 mM sodium pyruvate. For costaining and multiplexed FLIM-PLIM experiments, we used the following additional probes: Pt-Glc (2 μM, 1 h), TMRM (10 nM, 0.5 h), and Nile red (1 μg/mL, 1 h). For VD3 treatment, organoids were incubated with 100 nM for 3 days prior to measurements. For titration, EGTA was added sequentially at final concentrations 0.5 and 2.5 mM. The solution of EGTA (45 mM) was prepared from the original 450 mM stock solution, pH 8.0, with tenfold dilution in the imaging media.

FLIM Microscopy. Confocal FLIM was performed on a custom-made upright Zeiss Axio Examiner Z1 upright laser-scanning FLIM-PLIM microscope as described previously.[25,49] The microscope was equipped with 5×/0.25 Fluar air, 20×/1.0 and 63×/1.0 W-Plan Apochromat water-dipping objectives, integrated *T* and *Z*-axis controls, BDL-SMNI 405 and 488 nm pulsed diode lasers, DCS-120 confocal TCSPC scanner, photon counting detectors, and SPCM and SPCImage software (Becker&Hickl GmbH). Lgr5-GFP, Pt-Glc (PLIM), and TMRM (FLIM) probes were imaged as described previously,[49,50] Nile red was excited using 488 nm laser, and emission was collected at 512−536 nm ("green", Semrock) and 565−605 nm ("red") spectral channels. ColBD-Twitch was excited either with 405 nm (em. 446−486 nm, "Donor" fluorescence, Semrock) or with 488 nm (em. 512−536 nm, "Acceptor" fluorescence).

FLIM calibration experiments were typically performed using Matrigel stained with ColBD-Twitch in PBS or 0.135 mM NaCl supplemented with different concentrations of $CaCl_2$ and measured using a 5×/0.25 Fluar air objective (405 and 488 nm excitation).

Two-photon FLIM measurements were performed using an inverted Zeiss LSM 880 microscope (Zeiss, Jena, Germany) coupled with a Ti:Sapphire laser (Mai Tai HP; Spectra Physics, Santa Clara,

https://dx.doi.org/10.1021/acsabm.0c00649
ACS Appl. Bio Mater. 2020, 3, 5310−5321

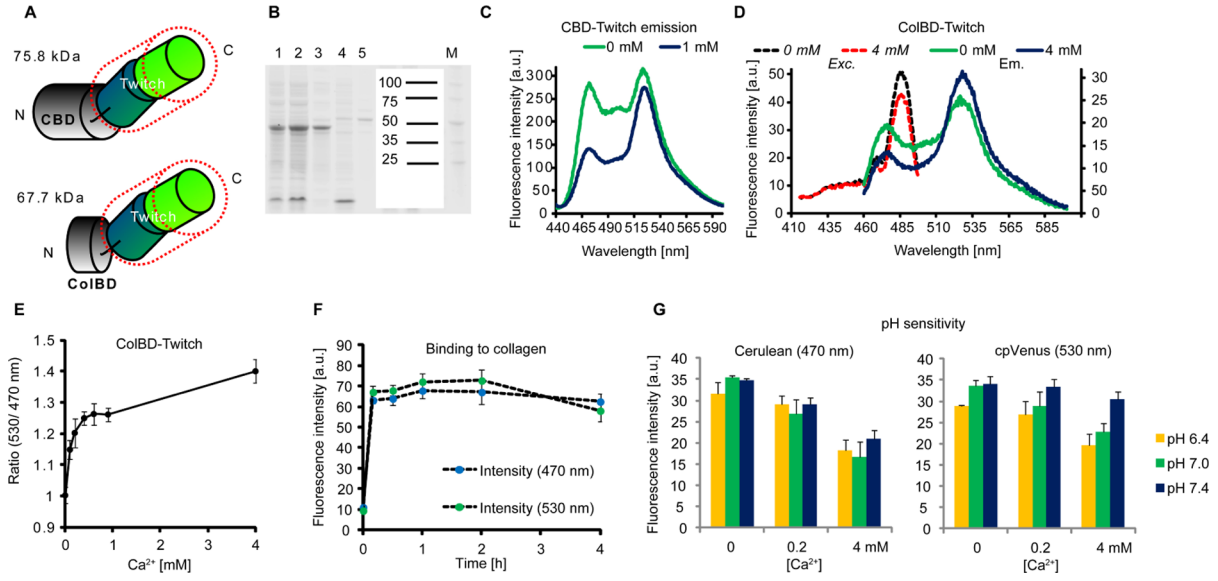

Figure 1. Design and initial evaluation of the cellulose (CBD)- and ColBD-tagged Twitch-2B 54S+ proteins. (A) Schematic structures of proteins. Positions of N (contain 6xHis sequences) and C-termini are indicated. (B) SDS-PAGE of ColBD-Twitch (1—total bacterial lysate, 2—cleared lysate, and 3—purified protein) and CBD-Twitch (4—cleared bacterial lysate, 5—purified protein). Mw standards (kDa) are shown on the right. (C) Fluorescence emission of the purified CBD-Twitch protein (0.7 μM, 20 °C) in solutions with 0 and 1 mM $CaCl_2$. (D) Fluorescence excitation (dashed lines) and emission (solid lines) spectra of ColBD-Twitch at 0 and 4 mM $CaCl_2$ in solution, obtained on a microplate reader. (E) Ratiometric response of ColBD-Twitch fluorescence emission measured from 0 to 4 mM $CaCl_2$. $N = 3$. (F) Binding of collagen I-coated plates with 0.5 μM ColBD-Twitch (20 °C). (G) pH sensitivity of the ColBD-Twitch protein. The protein was diluted to 0.07 μM in buffers with different pH and concentrations of $CaCl_2$ as indicated and measured on a microplate reader at 470 (A), 530 nm (B), and in spectral emission scan modes. $N = 3$.

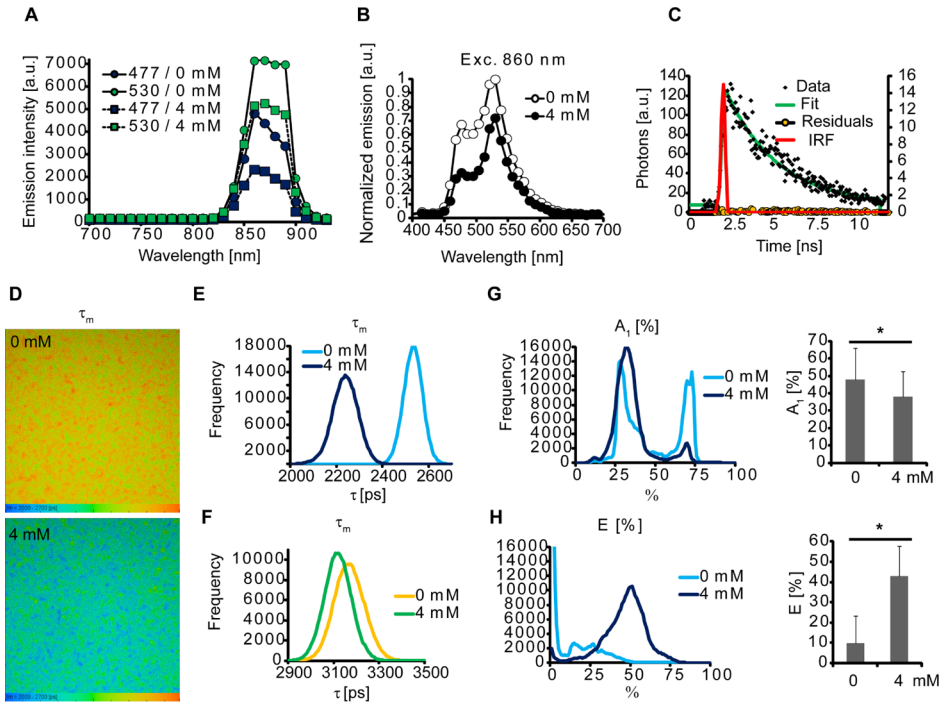

Figure 2. ColBD-Twitch protein biosensing properties under two-photon FLIM. ColBD-Twitch bound to Matrigel (1 μM, 1 h) was measured at 0 and 4 mM $CaCl_2$. (A,B) Two-photon excitation (A) and emission spectra (B). (C) Example of fluorescence decay (double exponential fitting) of ColBD-Twitch at 0 mM $CaCl_2$. (D) FLIM images (double-exponential fit, τ_m). (E,F) Fluorescence lifetime distribution histograms for donor (477 nm em., E) and acceptor (530 nm em., F) spectral channels. (G,H) FRET efficiency in the donor channel in response to Ca^{2+} expressed as A_1 [%] (G) and the FRET ratio (H). Asterisks indicate significant differences ($p = 0.001$, t-test). $N = 3$.

USA) and a two-channel "BIG 2.0" FLIM detector (Becker&Hickl GmbH). Images were collected with a 25×/0.8 NA objective (LCI Plan-Neofluar; Zeiss, Jena, Germany), 10% laser power, and a pixel dwell time of 16.38 μs. Two-photon excitation and emission curves were measured using the Lambda mode at a 8.5 nm channel resolution. FLIM measurements of DC celery scaffolds coated with collagen IV and stained with ColBD-Twitch were performed at 860 nm with a resolution of 256 × 256 pixels. The collected signal was separated by splitting into two channels, 460−500 nm for channel 1 and 520−560 for channel 2.

https://dx.doi.org/10.1021/acsabm.0c00649
ACS Appl. Bio Mater. 2020, 3, 5310−5321

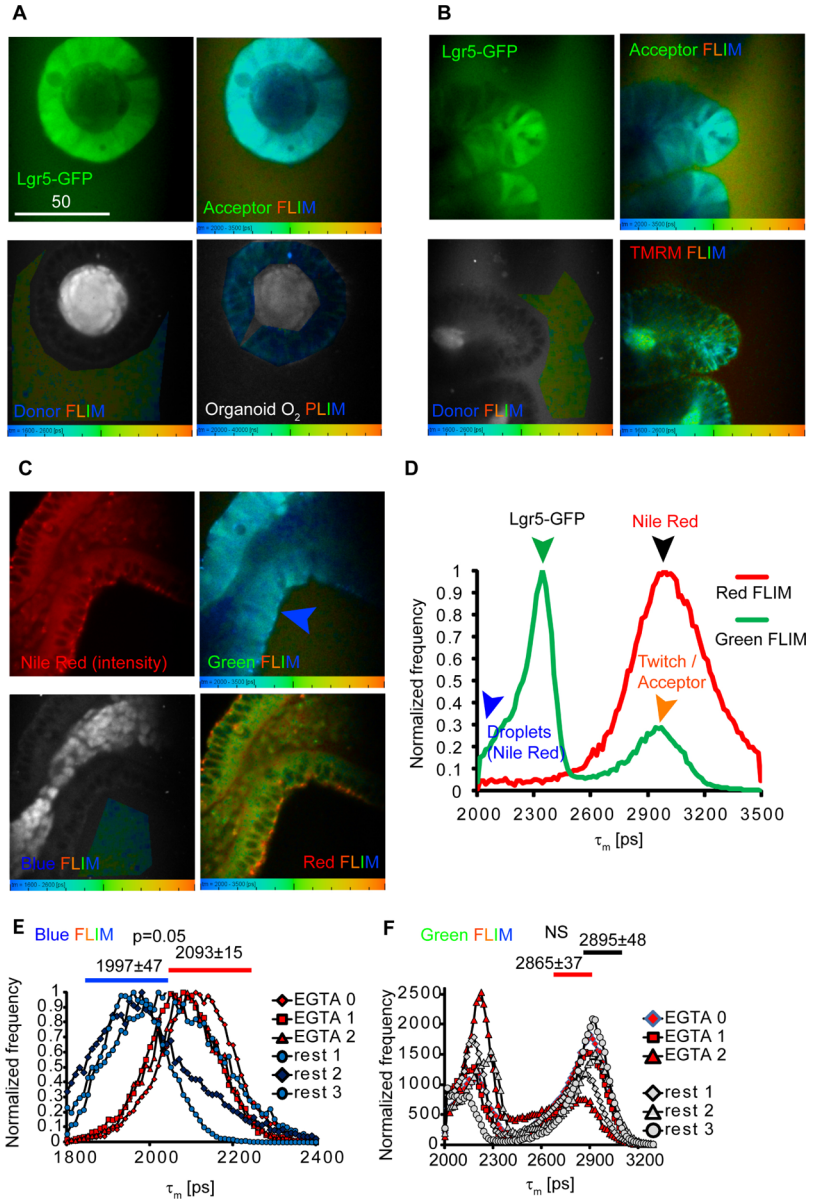

Figure 3. Multiparameter FLIM imaging of Matrigel stained with ColBD-Twitch in the culture of mouse intestinal Lgr5-GFP organoids. Organoids grown in ENR VC medium were stained with O_2 probe (Pt-Glc, 2 μM, 1 h), TMRM (10 nM, 1 h), or Nile red (1 μg/mL, 1 h). Matrigel was prestained with ColBD-Twitch (2 μM, 1 h) in complete growth medium prior to FLIM measurements. (A) Lgr5-GFP (green, intensity), O_2-PLIM (635−675 nm em.), ColBD-donor (blue, 470 nm em.), and acceptor (green, 530 nm em.) FLIM images showing stained Matrigel and GFP fluorescence lifetime. (B) Lgr5-GFP (green, intensity) and FLIM images showing the ColBD-donor, acceptor, and TMRM-FLIM (488 nm exc., 565−605 nm em.). (C,D) Nile red (intensity, 565−605 nm em.), green, blue (*i.e.* donor), and red FLIM images (C) and lifetime distribution histograms for respective green (512−536 nm) and red (565−605 nm) fluorescence emission channels for Nile red-stained organoid samples (D). Characteristic peaks of lifetimes for droplets in the green channel (basal membrane), GFP, and matrix are indicated by arrows. (E,F) Comparisons of blue and green FLIM distribution histograms for Nile red in VD3-stimulated (100 nM, 3 d) organoids in response to Ca^{2+} depletion (2.5 mM EGTA). Significant differences were observed only in the blue (donor) channel. N = 3. The scale bar is in μm.

Spectral and Plate Reader Measurements. Absorption and fluorescence spectra of CBD-Twitch and ColBD-Twitch in solution were collected on a 8453 diode array spectrophotometer (Agilent) and LS-50B (PerkinElmer) at room temperature as described previously.[25] Staining efficiency and ratiometric fluorescence measurements in solution and in collagen scaffolds were performed using the BMG Clariostar microplate reader (BMG Labtech Ltd, UK) equipped with the atmospheric control unit (CO_2, T, and O_2), monochromator, and MARS software.

Data Analysis and Statistics. Fitting of FLIM decays was performed using SPCImage software, essentially as described previously,[25,49] using mono- (phosphorescence lifetime imaging) and double-exponential decay fitting procedures (considering $\chi^2 < 1.5$ factor as appropriate). FRET efficiency and A1 (Figures 3 and 4) were calculated as E [%] = 1 − τ_1/τ_2 using SPCImage (Becker & Hickl) software.

Typically, fitting was tested for few separately taken pixels and applied to the whole 256 × 256 (or 512 × 512) image. Lifetime frequency distribution histograms were used for the chosen image regions (*e.g.* areas with Matrigel or basal membrane-localized lipid droplets) and used for further analysis. The peak values (identified using the integration function in Origin software) were tested for normality of distribution (Shapiro−Wilk test) and evaluated for statistical significance of differences using the *t*-test (normal

https://dx.doi.org/10.1021/acsabm.0c00649
ACS Appl. Bio Mater. 2020, 3, 5310−5321

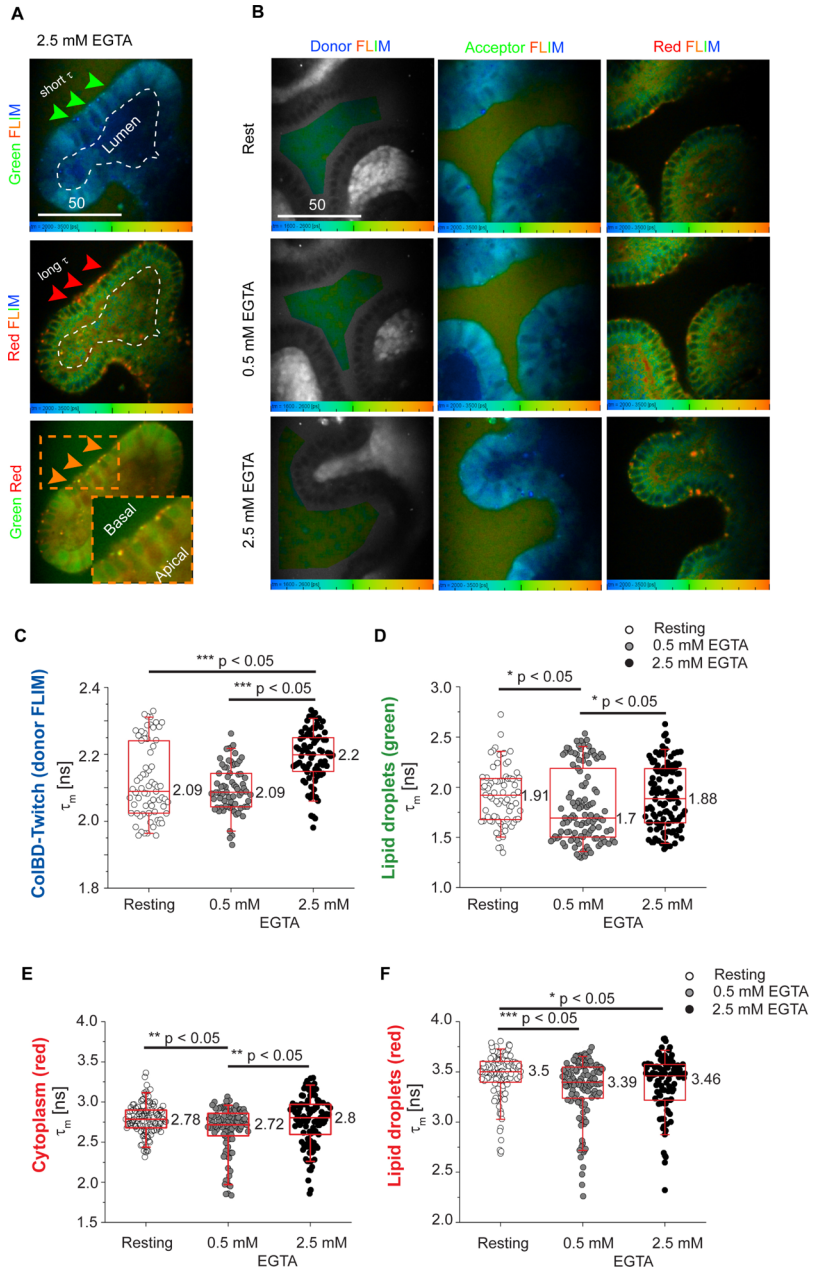

Figure 4. Multiparameter FLIM of extracellular Ca^{2+} and lipid droplets in live mouse Lgr5-GFP intestinal organoids. (A) Basal membrane localization of Nile red-stained lipid droplets in organoids. Green (512−536 nm em.) and red (565−605 nm em.) FLIM and combined intensity green/red images are shown. Droplets are indicated by arrows. Lumen is indicated by a white dashed line. (B) Examples of spectrally resolved (donor, 446−486 nm em., acceptor, 512−536 nm em. and red channel, 565−605 nm em.) FLIM images of Nile red-stained Lgr5-GFP organoids and ColBD-Twitch-stained Matrigel matrix at rest and after sequential addition of EGTA (5 min). (C−F) "General statistical analysis" of fluorescence lifetimes for the donor FLIM channel (Matrix) measured with ColBD-Twitch, cytoplasmic (red), green, and red spectral droplet fractions of Nile red measured and calculated at rest and different concentrations of EGTA (first experiment). The data points correspond to the average lifetime values calculated from ROIs taken from seven organoid images per each condition. *P* values indicate statistical significance (Mann−Whitney test): $*p < 0.05$, $**p < 0.005$ and $***p < 0.0005$. Box charts correspond to the median (values shown in numbers), 25 and 75 percentiles. Whiskers show 5 and 95 percentiles. The scale bar is in μm.

distribution) or Mann−Whitney tests appropriately. For detailed analysis of fluorescence lifetime changes, the *XY* (512 × 512) photon intensity and calculated FLIM data matrices were exported as ASCII files, opened in Microsoft Excel, and visualized using "conditional formatting". This allowed choosing individual ROIs relevant to Matrigel (5 × 5 pxl), lipid droplets, or cytoplasmic/membrane areas (2 × 2 pxl) and applying for the fluorescence lifetime data. Average fluorescence lifetime values for separate ROIs were then used for the statistical analysis (Figures 4, 5, and S7), as described previously.[51]

The titration of Matrigel/intestinal organoids with EGTA was performed twice, using cultures from different passages (Figures 4, 5, and S7). Each of the experimental replicate consisted of two independent treatments; thus, four independent treatments were performed for EGTA experiment. For "general statistical analysis", we compared the data collected from all microscopy images corresponding to each treatment, and the measurements performed on different organoid passages were analyzed separately (Figures 4C−F and S7). ROIs of the same size corresponding to the independent lipid droplets (for green or red spectral channels of Nile red) or labeled Matrigel

https://dx.doi.org/10.1021/acsabm.0c00649
ACS Appl. Bio Mater. 2020, 3, 5310−5321

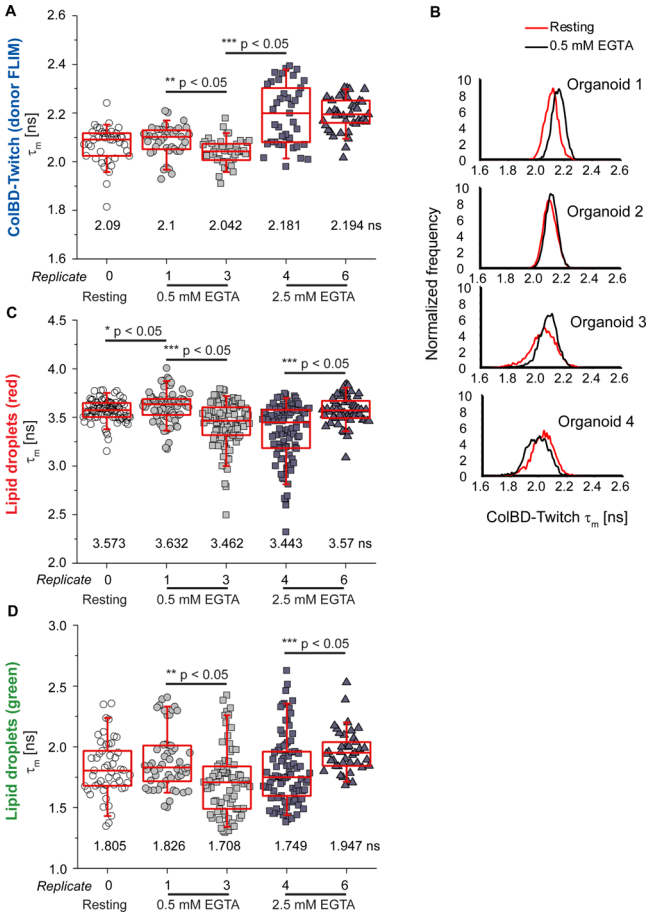

Figure 5. "Time-dependent analysis" of changes of fluorescence lifetimes for the donor FLIM channel (ColBD)-Twitch/Matrix (A) and different spectral fractions of Nile red (C,D) in response to addition of EGTA. Data combined from the two independent experiments represent average lifetime values calculated from ROIs taken from four organoid images per each condition. *P* values indicate statistical significance (Mann−Whitney test): $*p < 0.05$, $**p < 0.005$, and $***p < 0.0005$. Box charts correspond to the median (values shown in numbers), 25 and 75 percentiles. Whiskers show 5 and 95 percentiles. (B): Fluorescence lifetime distribution histograms of individual organoids at rest and immediately after addition of 0.5 mM EGTA for different ColBD-Twitch-stained Matrigel areas.

areas (blue spectral channel of ColBD-Twitch) collected from independent microscopy images were assumed as individual statistical units. A set of data for each experimental condition was analyzed for normality of distribution with the nonparametric Mann−Whitney test. For time-dependent analysis (Figure 5), we combined microscopy images of organoids from four independent treatments with EGTA and organized them into five groups (by four organoids in each group) according to the order of imaging (resting: organoids measured prior to the addition of 0.5 mM EGTA, 0.5 mM EGTA (1), and 2.5 mM EGTA (4); organoids measured immediately after addition of EGTA, 0.5 mM EGTA (3), and 2.5 mM EGTA (6); and organoids measured 7−8 min after addition of EGTA) using ROIs collected from these images as statistical units, as described above.

RESULTS

Cloning, Production, and Initial Evaluation of CBD-Twitch and ColBD-Twitch Proteins. Our preliminary research has highlighted the potential for design of scaffold-binding recombinant proteins consisting of the CBD with pH (ECFP) or Ca^{2+}-sensing (GCaMP2) proteins.[25] Here, we looked at Twitch-2B 54S+ mutant,[44] further referred simply as "Twitch", which is based on Cerulean and cpVenus proteins, and a minimal Ca^{2+}-binding domain which displays low affinity promising for extracellular measurements (Figure 1A). We produced chimeras of Twitch fused with cellulose- and collagen[52]-binding domains in bacteria and found that CBD-Twitch showed folding and maturation rates similar to CBD-ECFP (yields of ∼7 mg/L of culture when expressed at 4 °C). In contrast, the ColBD-Twitch protein having a short vWF peptide demonstrated higher yields of the folded protein, achieving >50−70% folding rates and a yield of >60 mg/L of culture. SDS-PAGE confirmed integrity and purity of the produced proteins, although CBD-Twitch displayed the presence of the second electrophoretic band (Figure 1B), not affected by expression conditions in the presence of protease inhibitors (not shown). Purified CBD-Twitch and ColBD-Twitch showed very similar Ca^{2+}-sensitivity in solution with ∼1.4 or higher ratiometric response to Ca^{2+} (Figure 1C−E). ColBD-Twitch showed rapid binding of collagen I-coated microplates, requiring only 15−20 min of the incubation time and confirming functional activity of the vWF peptide (Figure 1F). Our preliminary tests also confirmed binding activity of the proteins toward cellulose (nanofibrillar and DC scaffolds, CBD-Twitch) and collagen (Matrigel, collagen I, IV, and DC pericardial tissue, ColBD-Twitch) (not shown).

Because the pH-sensitivity is a well-known issue with fluorescent proteins,[53] we investigated effects of pH on the Ca^{2+}—sensitivity of the ColBD-Twitch protein (Figures 1G and S1). Comparison of fluorescence intensity for blue (Cerulean) and green (cpVenus) spectral channels at three different Ca^{2+} concentrations showed that low pH (pH 6.4) significantly affected fluorescence in the green channel, thus influencing the ratiometric response. While the physiological range of pH 7−7.4 showed minimal influence of Ca^{2+}—sensitivity, we suggest that pH control and monitoring have to be used with this biosensor in the intensity-based detection.

We also looked at the stability of the produced biosensor. Thus, we analyzed response to Ca^{2+} for the ColBD-Twitch sample stored over 14 days at 4 °C (Figure S2). We detected decreased stability of green channel fluorescence (cpVenus protein) and change of ratio, resulting in decreased performance for the stored protein.

Biosensing Properties of Twitch Proteins in One- and Two-Photon Excited FLIM. The design of the Twitch biosensor implies Ca^{2+}-dependent FRET between Cerulean (donor, blue fluorescence) and cpVenus (acceptor, green fluorescence) proteins, both of which can potentially display changes of the fluorescence lifetime. To understand this phenomenon, we stained the Matrigel matrix with ColBD-Twitch and analyzed fluorescence lifetimes using two-photon and one-photon excited "confocal" FLIM modalities (Figures 3 and S3).

Analysis of two-photon excitation and emission spectra demonstrated differences in Ca^{2+}-dependent responses for donor and acceptor proteins within a Twitch biosensor, with optimal excitation in the range of 860−890 nm (Figure 2A). Ca^{2+}-dependent changes in the ratiometric intensity mode (Figure 2A,B) confirmed solution-based measurements (Figure 1). In the FLIM mode, we saw changes in τ_m (donor channel) and observed lifetime changes (τ_m decreasing from ∼2.5 to 2 ns or lower upon binding Ca^{2+}) comparable to confocal FLIM data (Figure S3). The multiexponential character of the donor fluorescence lifetime was also confirmed by phasor analysis

https://dx.doi.org/10.1021/acsabm.0c00649
ACS Appl. Bio Mater. 2020, 3, 5310−5321

(Figure S3C). Interestingly, acceptor fluorescence did not reveal drastic changes upon Ca^{2+} binding (Figure 2F).

We also observed Ca^{2+}-dependent changes in the *A*1 [%] fraction and more profound changes in FRET efficiency in the two-photon mode (Figure 2G,H). Thus, the ColBD-Twitch protein showed well-resolved changes of the fluorescence lifetime of the FRET donor part (blue emitting Cerulean) to changing Ca^{2+} concentrations over the range of 0−4 mM. The double-exponential nature of the fluorescence decay obeyed expected FRET donor mechanics, leading to a decrease in the fluorescence lifetime (due to transfer of energy to the acceptor) upon binding of Ca^{2+}, bringing Cerulean and cpVenus to the FRET distance. These data are in agreement with those previously reported for Cerulean-based Ca^{2+}-sensors and suggest that ColBD-Twitch bound to the collagen-containing matrix can be used as a Ca^{2+} biosensor.

To further understand the characteristics of the Twitch biosensor with the other types of scaffolds, we performed additional confocal FLIM experiments. First, we produced the DC plant tissue celery scaffold[25] and labeled it with the CBD-Twitch protein. After observing specific binding, we incubated the scaffold with different Ca^{2+} concentrations, and using FLIM microscope, we detected changes in τ_m very similar to those obtained with ColBD-Twitch bound to Matrigel, having ∼2−2.6 ns range of lifetimes for 4−0.05 mM, respectively (Figure S4). In another experiment, we coated the DC celery scaffold with collagen IV and labeled it with the ColBD-Twitch protein (Figure S5). We found that the scaffold displayed a slightly different staining pattern than that observed with CBD-Twitch on the uncoated (pure cellulose) matrix, showing fluorescent signals from the scaffold cavities. This phenomenon could be a result of collagen coating of the scaffold and the difference in binding between cellulose- and ColBD proteins. Still, when we analyzed these regions stained with ColBD-Twitch, we also saw expected dynamics of fluorescence lifetime changes. This confirms that ColBD-Twitch can be used with collagen-based scaffolds other than Matrigel (Figure S5).

Collectively, the Twitch biosensor fused with either CBD or ColBD domains could bind respective cellulose or collagen-based scaffolds and display biosensing properties suitable for confocal and two-photon excited FLIM measurements.

Evaluation of the ColBD-Twitch Protein in Multi-Parameter FLIM Measurements with the Live Culture of Mouse Intestinal Organoids. Observed spectral and photophysical properties of the Twitch biosensor prompted us to test it in a spectrally and lifetime-resolved FLIM measurements with a relevant 3D cell model. We chose the mouse Lgr5-GFP small intestinal organoid model,[54] which enables live tracing of stem (Lgr5-GFP$^+$) and differentiated enterocyte cells, grows in the Matrigel matrix, and recapitulates most of the functions of the native epithelium.[55] Mouse intestinal organoids have been already extensively evaluated in a number of FLIM and PLIM assays, informing on cell oxygenation, proliferation, mitochondrial polarization, redox status, and others.[25,49,50,56,57] Although in the previous work we have demonstrated pH-FLIM imaging of organoids combined with O_2 imaging, we were not able to measure acidification directly in Matrigel and assess extracellular Ca^{2+}.[25]

First, we tested if we could combine Matrigel-based Ca^{2+} sensing *via* ColBD-Twitch labeling with other FLIM and PLIM assays (Figure 3). In this experiment, we collected fluorescence signals from Matrigel in blue (donor) and green (acceptor) spectral channels for the ColBD-Twitch protein and green fluorescence from Lgr5-GFP regions in organoids. We also expected that in addition to GFP ($\tau \sim 2.4$ ns), the FLIM method would enable measuring other green dyes and biosensors because of the possibility of separation in the lifetime ("time") domain.

Thus, we successfully imaged live organoid oxygenation in such a setup, using the blue-excited red-emitting phosphorescent O_2 probe, which has lifetimes in the range of 20−57 μs[57] (Figure 3A). With the TMRM dye, which labels polarized mitochondria and shows membrane polarization-dependence of fluorescence lifetimes,[50] we gathered information on GFP distribution, heterogeneous mitochondrial polarization, and ColBD-Twitch-labeled Matrigel scaffolds (Figure 3B) in agreement with previous findings.[50]

Next, we chose Nile red, which is a frequently used probe for assessment of lipids and lipid droplets; note that it also shows Ca^{2+}-sensitivity, for example, by detecting conformational changes of calmodulin upon binding Ca^{2+}[58] or by binding phospholipid/Ca^{2+} complexes.[59−61] In the presence of lipids and other amphiphilic molecules, Nile red displays both spectral (green/orange) and fluorescence lifetime changes. We tested if the green fluorescence of Nile red could potentially interfere with Lgr5-GFP signals (Figure 3C,D). While the fluorescence intensity signals in the green channel (512−536 nm em., exc. 488 nm) overlapped, the lifetimes were distinguishable on a frequency lifetime distribution histogram (Figure 3D "green"), showing three areas of lifetime distribution: <2.1 ns for basal membrane-localized droplets, ∼2.3−2.4 ns for Lgr5-GFP, and ∼3 ns peak for Matrigel labeled with ColBD-Twitch acceptor fluorescence. In contrast, Nile red fluorescence in the red channel (565−605 nm, "red FLIM") demonstrated the single peak of overlapping lifetimes over a range of 2.6−3.5 ns, corresponding to the membrane, cytoplasmic (shorter lifetimes in 2.6−3 ns range), and lipid droplet (generally longer lifetimes in 2.8−3.5 ns range) staining (Figure 3C,D red).

In a proof-of-principle experiment, we tested responses of the donor (blue) and acceptor (green) fluorescent forms of Matrigel-bound ColBD-Twitch to the depletion of extracellular Ca^{2+} upon chelation with 2.5 mM EGTA. In agreement with calibration experiments (Figures 2 and S3−S5), the donor channel demonstrated the most striking response to Ca^{2+} depletion (Figure 3E,F).

Thus, staining of organoids with Nile red allowed identification of a fraction of basal membrane-localized lipid droplets, seen in both green and red spectral channels (Figures 3 and S6). Pretreatment with 1α, 25$(OH)_2$-vitamin D3 (VD3) affected both fluorescence lifetimes of Nile red cytoplasmic and membrane-stained structures and increased the number of lipid droplets in organoids (Figure S6). This effect supports the previous report on the effect of VD3 on lipid metabolism in the intestine[62] and suggests that VD3 upregulates Ca^{2+} metabolism.[63] We then decided to investigate how the changes in extracellular Ca^{2+} could affect Nile red fluorescence in the intestinal organoids.

We found that basal membrane-localized lipid droplets seen in different spectral channels did not fully colocalize, and their fluorescence lifetimes tended to be different (Figure 4A). We hypothesized that such droplets were of a similar type, but the different lifetimes and spectral characteristics could indicate differences in labeling of their content by Nile red. The short lifetimes in the green channel can reflect the labeling of neutral lipid cores (mainly triacylglycerol and sterol esters) of lipid

https://dx.doi.org/10.1021/acsabm.0c00649
ACS Appl. Bio Mater. 2020, 3, 5310−5321

droplets, while longer red fluorescence lifetimes can correspond to both the core and polar monolayers consisting of phospholipids and lipid droplet-associated proteins.[58,64]

We performed the sequential addition of 0.5 and 2.5 mM EGTA and analyzed fluorescence lifetimes for Matrigel/ColBD-Twitch (blue channel) and for Nile red (green and red channels) (Figure 4B).

First, we found that ColBD-Twitch did not detect statistically significant changes (Figure 4C) or detected decrease (Figure S7A) rather than expected increase of the donor fluorescence lifetime between resting (0 mM EGTA) and 0.5 mM EGTA concentrations. However, we saw significant changes at 2.5 mM EGTA in both experimental replicates, demonstrating the increase of a donor fluorescence lifetime, that is, the decrease of FRET (Figures 4C and S7A).

Interestingly, analysis of Nile red-stained droplets (green and red spectral channels, Figure 4D,F) and membrane/cytoplasmic Nile red signals (Figure 4E) showed significant response to Ca^{2+} depletion already after addition of 0.5 mM EGTA. These results were not reproduced in the second experimental replicate (Figure S7B,C) but showed the same tendencies. Thus, sequential chelation of external Ca^{2+} affected Nile red fluorescence, clearly demonstrating changes in the intracellular environment. This is likely due to the conformational reorganization of the lipid membrane and protein structures in the cytoplasm.

In order to address the variability in Nile red fluorescence lifetime response and understand why ColBD-Twitch demonstrated an increase rather than the decrease of free extracellular Ca^{2+} after addition of 0.5 mM EGTA to the organoids, we performed "time-dependent analysis" of the fluorescence lifetime time changes (Figure 5, see Experimental Section for details). This enabled us to detect very minor changes in lifetime values, which were not detectable by the "general statistical analysis", combining all the time points for each treatment.

Analysis of time-dependent changes for ColBD-Twitch demonstrated the initial growth of fluorescence lifetimes after the first EGTA addition, reflecting decrease of the extracellular Ca^{2+} concentration (Figure 5A). These changes were visible on lifetime distribution histograms for most organoids in the group (Figure 5B). Such response of ColBD-Twitch accompanied the increased number of lipid droplets with longer fluorescence lifetimes in red and green spectral channels (Figure 5C,D). In contrast, organoids measured 7−8 min later after the first addition of EGTA displayed statistically significant decrease of ColBD-Twitch fluorescence lifetimes accompanied by the corresponding changes of Nile red lipid droplet fluorescence (red and green channel) (Figure 5A,C,D). Such a "drop" of fluorescence lifetimes explains why we detected almost no changes or statistical decrease of ColBD-Twitch and Nile red lifetime values using the "general statistical analysis" approach (Figures 4C−F and S7). This phenomenon can be explained by the ability of cells in organoids to regulate extracellular Ca^{2+} *via* control of the Ca^{2+} efflux. In this case, the concomitant changes in the Nile red fluorescence lifetimes provide indirect evidence for such regulation. Further addition of EGTA led to the statistically significant increase of ColBD-Twitch fluorescence lifetime values due to the decrease of free extracellular Ca^{2+} (Figure 5A), which correlated with slowly evolving increase of the lipid droplet fluorescence lifetime in green and red spectral channels (Figure 5C,D). Although we did not observe a further increase of the fluorescence lifetime after the second addition of EGTA with ColBD-Twitch, the cells could still attempt restoring balance of chelated extracellular Ca^{2+}: the delayed response of Nile red fluorescence could be viewed as evidence of activation of the intracellular Ca^{2+} pools in response to addition of 2.5 mM EGTA.

To rule out the buffering capacity of Matrigel in Ca^{2+} sequestering, we performed the control experiment, where we treated organoid-free Matrigel with the sequential addition of EGTA (Figure 6). Thus, we confirmed the specific "decrease" of ColBD-Twitch lifetimes (Figures 4 and 5), reflecting the active role of the intestinal epithelium in compensating extracellular Ca^{2+} chelation.

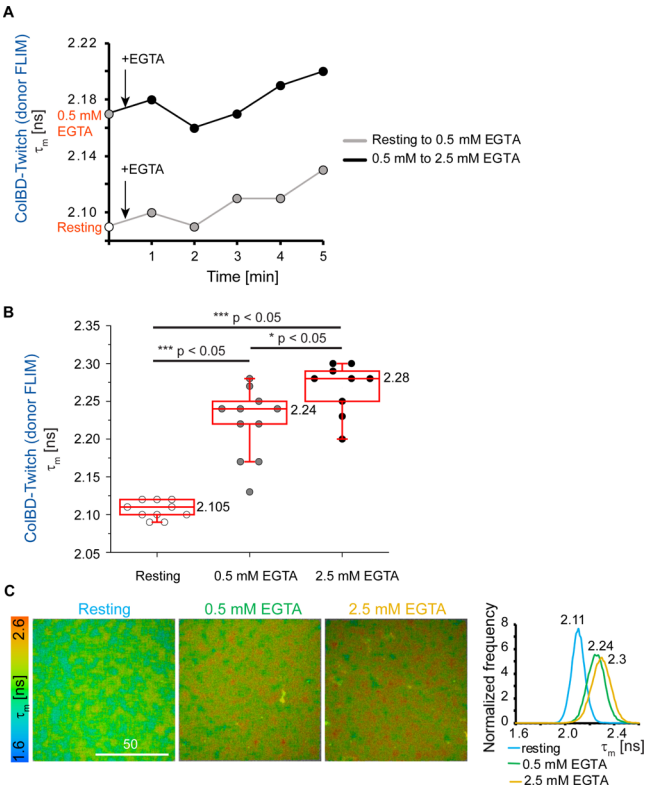

Figure 6. Changes in the fluorescence lifetime for ColBD-Twitch bound to the Matrigel and treated with EGTA in the absence of organoids. (A) Time-dependent changes of ColBD-Twitch (donor)-stained Matrigel. The kinetical profiles are shown for two independent ROIs. Data correspond to the peak values of distribution histograms measured for the same ROI prior to addition of EGTA (resting or 0.5 mM EGTA) and at different time points. (B) General statistical analysis of fluorescence lifetimes at rest and after adding 0.5 and 2.5 mM EGTA. Data correspond to the peak values of the fluorescence lifetime distribution histograms for different ROIs measured at rest and after EGTA addition. *P* values indicate statistical significance (Mann−Whitney test): $*p < 0.05$, $**p < 0.005$ and $***p < 0.0005$. Box charts correspond to the median (values shown in numbers), 25 and 75 percentiles. Whiskers show 5 and 95 percentiles. (C) Examples of FLIM images of stained Matrigel and their corresponding distribution histograms. The scale bar is in μm.

DISCUSSION

Here, we describe design and application of the extracellular Ca^{2+}-sensing fluorescent protein, which provides labeling of the extracellular matrices for measurements in 3D tissue models and in related *in vivo* settings. While the sensing

https://dx.doi.org/10.1021/acsabm.0c00649
ACS Appl. Bio Mater. 2020, 3, 5310−5321

principle representing the binding domain combined with fluorescent protein biosensors is not new,[25] this is the first use of FRET-FLIM biosensors as a collagen-based scaffold biosensor in a successful application. Recombinant cellulose- and ColBD-based Twitch-2B chimeras showed high expression yields (7−60 mg/L culture) and efficient folding when expressed in bacteria, especially in case of the ColBD-Twitch protein fused to the short vWF peptide. Thus, we achieved improved production and demonstrated versatility of the approach suggesting that matrix-binding polypeptides can be employed for diverse types of scaffolds and related applications.

We found that the binding domain attached to Twitch-2B displayed minimal or no negative effects on the performance of the biosensor in a ratiometric mode, which makes it similar to other related biosensors.[44] On the other hand, Ca^{2+}-sensitivity in a fluorescence lifetime domain has not been studied before for the Twitch proteins: as expected with similar types of FRET-FLIM biosensors,[20,43,45] donor fluorescence decay displayed double-exponential decay, with Ca^{2+}-dependent changes in the A1 fraction and FRET efficiency. Thus, Ca^{2+}-calibration can be realized in units of mean lifetime τ_m (double-exponential fit), A_1 [%], FRET efficiency, and by other means. In case of ColBD-Twitch, we found τ_m as the most useful readout, reflecting robust and reproducible changes in response to Ca^{2+}, under one- and two-photon excitation modes (Figures 2 and S3). On the other hand, the acceptor fluorescence lifetime did not show reliable changes in response to Ca^{2+} (Figure 2). We explain this by less efficient energy transfer from Cerulean to cpVenus because of differences in the protein microenvironment such as pH, leading to dissipation of the energy or the stability of cpVenus as the acceptor. Indirectly, these data point at FLIM as a preferred readout for quantitative measurements with Twitch-2B 54S+ rather than the ratiometric intensity. This can be different from the situation with the endogenously expressed biosensor when its stability is not so strongly dependent on the environment and it is continuously synthesized and degraded by the cell.[44]

Using of the vWF peptide for labeling collagen scaffolds also suggests that biosensor binding to Matrigel and related matrices can potentially compete with the Ca^{2+}-sensing osteonectin/SPARC protein,[65] which is known to be present in the Engelbreth−Holm−Swarm tumor.[66] Therefore, it would be very interesting to test other ColBDs for targeting Twitch or related biosensors to understand their binding and biosensing properties when bound to the Matrigel matrix, especially their influence by the Ca^{2+}-dependent conformational changes of the scaffold.

Sensing in a fluorescence lifetime domain provides more options for spectral and lifetime-based multiplexing, and we demonstrated compatibility of Ca^{2+}-FLIM by ColBD-Twitch with assays measuring cell oxygenation (O_2-PLIM) and mitochondrial polarization (TMRM-FLIM) and analyzing lipids and lipid droplets (Nile red-based FLIM) using the stem cell-derived Lgr5-GFP mouse small intestinal organoid model (Figures 3−6).

Generally, analysis of extracellular dynamic microgradients of Ca^{2+} using *in vitro* models is expected to have limited application potential. However, in our model, we saw measurable changes of Ca^{2+} in the solution surrounding the scaffold in DC collagen-coated cellulose and in Matrigel matrices. We did not detect subtle differences in Ca^{2+} gradients surrounding organoids because of nonperfect optical sectioning and rather slow and equilibrium-based measurements occurring within minutes. We also showed usefulness of the sensor for combined measurements of Ca^{2+}-dependent changes of lipid droplets with Nile red. By using ColBD-Twitch as a reference marker of Ca^{2+} depletion, we observed dynamic changes in lipid droplet organization potentially linked to the local polarity changes of lipid structures detected by Nile red (Figures 4 and 5). These changes were correlated with extracellular Ca^{2+} fluctuations showing that extra- and intracellular Ca^{2+} pools were in close connection with each other. It should be kept in mind that use of Nile red does not discriminate between fluctuations of free Ca^{2+} and Ca^{2+} bound to the phospholipids. As Ca^{2+}-signaling regulates many different cellular functions in a wide temporal and concentration ranges, the intracellular fluctuations of free Ca^{2+} are strictly regulated and sequestered in the organelles or the extracellular environment.[16] Potentially, the observed changes in lipid droplets and cytoplasmic fractions of Nile red were caused by Ca^{2+} binding to the lipid droplets and cellular membranes, which could act as additional depots in cells of the intestinal epithelium, similar to cardiomyocytes and neuroepithelial and immune cells.[60,61,67] If this is the case, lipid droplets can play a role in rapid restoration and maintenance of the external Ca^{2+} pool.

Our data provide basis for future study of processes of lipid and Ca^{2+} metabolism in the intestinal organoids; the logical next step would be a more detailed analysis of droplets and Ca^{2+} dynamics by comparing kinetical (<1 s) and equilibrium responses. The performed extracellular Ca^{2+} analysis would benefit from parallel measurement of intracellular Ca^{2+} in intestinal organoids, but we did not perform these measurements using the Oregon Green BAPTA-1 FLIM probe[68] here, as we found that it did not stain Lgr5-GFP organoids embedded in Matrigel.

Importantly, the observed performance of cellulose and ColBD Twitch-2B biosensors highlights their potential for advanced *in vivo* and *ex vivo* measurements, such as microinjection in live zebrafish or mouse tissues such as cartilage, bone marrow, and intestine. When mixed with collagen or cellulose-based matrices, these biosensors can also be highly useful for *ex vivo* analysis of tumor organoids, wound healing studies, or more complex stem cell-derived organoid models.

■ ASSOCIATED CONTENT

Supporting Information

The Supporting Information is available free of charge at https://pubs.acs.org/doi/10.1021/acsabm.0c00649.

pH sensitivity of the ColBD-Twitch protein; storage stability of the ColBD-Twitch protein; biosensing properties of ColBD-Twitch protein measured on a confocal FLIM microscope; and additional general statistical analysis (PDF)

■ AUTHOR INFORMATION

Corresponding Author

Ruslan I. Dmitriev − *Metabolic Imaging Group, Laboratory of Biophysics and Bioanalysis, ABCRF, University College Cork, Cork T12 YN60, Ireland; I.M. Sechenov First Moscow State University, Institute for Regenerative Medicine, Moscow 119992, Russian Federation; Tissue Engineering and Biomaterials*

https://dx.doi.org/10.1021/acsabm.0c00649
ACS Appl. Bio Mater. 2020, 3, 5310−5321

Group, Department of Human Structure and Repair, Faculty of Medicine and Health Sciences, Ghent University, Ghent 9000, Belgium; orcid.org/0000-0002-0347-8718; Phone: 021-4901699; Email: r.dmitriev@ucc.ie, Ruslan.Dmitriev@UGent.be

Authors

Irina A. Okkelman − *Metabolic Imaging Group, Laboratory of Biophysics and Bioanalysis, ABCRF, University College Cork, Cork T12 YN60, Ireland*

Ryan McGarrigle − *Agilent Technologies Ireland Limited, T45 WK12 Cork, Ireland*

Shane O'Carroll − *Metabolic Imaging Group, Laboratory of Biophysics and Bioanalysis, ABCRF, University College Cork, Cork T12 YN60, Ireland*

Daniel Carvajal Berrio − *Department of Women's Health, Research Institute for Women's Health and Cluster of Excellence iFIT (EXC 2180) "Image-Guided and Functionally Instructed Tumor Therapies" (iFIT), Eberhard Karls University Tübingen, Tübingen 72074, Germany*

Katja Schenke-Layland − *Department of Women's Health, Research Institute for Women's Health and Cluster of Excellence iFIT (EXC 2180) "Image-Guided and Functionally Instructed Tumor Therapies" (iFIT), Eberhard Karls University Tübingen, Tübingen 72074, Germany; NMI Natural and Medical Sciences Institute at the University of Tübingen, Reutlingen 72770, Germany; Department of Medicine/Cardiology, Cardiovascular Research Laboratories, David Geffen School of Medicine at UCLA, Los Angeles 90095, California, United States*

James Hynes − *Agilent Technologies Ireland Limited, T45 WK12 Cork, Ireland*

Complete contact information is available at: https://pubs.acs.org/10.1021/acsabm.0c00649

Notes

The authors declare no competing financial interest.

■ ACKNOWLEDGMENTS

This work was supported by the Science Foundation Ireland (SFI) grant 18/IF/6238 and the Russian Science Foundation (RSF) grant 18-15-00407 ("production of scaffolds" part). We are grateful to Prof. O. Griesbeck (Max Plank University) for providing the Twitch-2B 54S+ expression construct and Dr. E. Grebenik (Sechenov University, Institute for Regenerative Medicine, Moscow) for providing the Collagen-Chitosan matrix for the initial tests and to Prof. D. Papkovsky (University College Cork) for providing the access to the FLIM microscope.

■ REFERENCES

(1) Brassard, J. A.; Lutolf, M. P. Engineering stem cell self-organization to build better organoids. *Cell Stem Cell* **2019**, *24*, 860−876.

(2) Ham, T. R.; Collins, K. L.; Hoffman, B. D. Molecular tension sensors: moving beyond force. *Curr. Opin. Biomed. Eng.* **2019**, *12*, 83−94.

(3) Badylak, S. F. The extracellular matrix as a scaffold for tissue reconstruction. *Seminars in Cell & Developmental Biology*; Elsevier, 2002; Vol. *13*, pp 377−383.

(4) Schilling, K.; El Khatib, M.; Plunkett, S.; Xue, J.; Xia, Y.; Vinogradov, S. A.; Brown, E.; Zhang, X. Electrospun Fiber Mesh for High-Resolution Measurements of Oxygen Tension in Cranial Bone Defect Repair. *ACS Appl. Mater. Interfaces* **2019**, *11*, 33548−33558.

(5) Ronaldson-Bouchard, K.; Ma, S. P.; Yeager, K.; Chen, T.; Song, L.; Sirabella, D.; Morikawa, K.; Teles, D.; Yazawa, M.; Vunjak-Novakovic, G. Advanced maturation of human cardiac tissue grown from pluripotent stem cells. *Nature* **2018**, *556*, 239.

(6) Breitwieser, G. E. Extracellular calcium as an integrator of tissue function. *Int. J. Biochem. Cell Biol.* **2008**, *40*, 1467−1480.

(7) Brown, E. M.; MacLeod, R. J. Extracellular calcium sensing and extracellular calcium signaling. *Physiol. Rev.* **2001**, *81*, 239−297.

(8) Gronthos, S.; Simmons, P. J.; Graves, S. E.; Robey, P. G. Integrin-mediated interactions between human bone marrow stromal precursor cells and the extracellular matrix. *Bone* **2001**, *28*, 174−181.

(9) Forsberg, M.; Seth, H.; Björefeldt, A.; Lyckenvik, T.; Andersson, M.; Wasling, P.; Zetterberg, H.; Hanse, E. Ionized calcium in human cerebrospinal fluid and its influence on intrinsic and synaptic excitability of hippocampal pyramidal neurons in the rat. *J. Neurochem.* **2019**, *149*, 452−470.

(10) Yang, H.; Curinga, G.; Giachelli, C. M. Elevated extracellular calcium levels induce smooth muscle cell matrix mineralization in vitro. *Kidney Int.* **2004**, *66*, 2293−2299.

(11) Lansdown, A. B. G. Calcium: a potential central regulator in wound healing in the skin. *Wound Repair Regen.* **2002**, *10*, 271−285.

(12) McNeil, P. L.; Steinhardt, R. A. Plasma membrane disruption: repair, prevention, adaptation. *Annu. Rev. Cell Dev. Biol.* **2003**, *19*, 697−731.

(13) Mansour, A. A.; Gonçalves, J. T.; Bloyd, C. W.; Li, H.; Fernandes, S.; Quang, D.; Johnston, S.; Parylak, S. L.; Jin, X.; Gage, F. H. An in vivo model of functional and vascularized human brain organoids. *Nat. Biotechnol.* **2018**, *36*, 432−441.

(14) Keren-Paz, A.; Cohen-Cymberknoh, M.; Kolodkin-Gal, D.; Karunker, I.; Dersch, S.; Wolf, S. G.; Olender, T.; Kartvelishvily, E.; Kapishnikov, S.; Green-Zelinger, P.; Shteinberg, M.; Zamir, G.; Gal, A.; Graumann, P.; Kerem, E.; Kolodkin-Gal, I. A novel calcium-concentrating compartment drives biofilm formation and persistent infections. *bioRxiv* **2020**, DOI: 10.1101/2020.01.08.898569.

(15) Nicholls, D. G. Mitochondria and calcium signaling. *Cell Calcium* **2005**, *38*, 311−317.

(16) Brini, M.; Carafoli, E. Calcium pumps in health and disease. *Physiol. Rev.* **2009**, *89*, 1341−1378.

(17) Vangheluwe, P.; Sepulveda, M. R.; Missiaen, L.; Raeymaekers, L.; Wuytack, F.; Vanoevelen, J. Intracellular Ca2+-and Mn2+-transport ATPases. *Chem. Rev.* **2009**, *109*, 4733−4759.

(18) Ziv, N. E.; Spira, M. E. Axotomy induces a transient and localized elevation of the free intracellular calcium concentration to the millimolar range. *J. Neurophysiol.* **1995**, *74*, 2625−2637.

(19) Han, S.; Tang, R.; Anderson, L. K.; Woerner, T. E.; Pei, Z.-M. A cell surface receptor mediates extracellular Ca2+ sensing in guard cells. *Nature* **2003**, *425*, 196−200.

(20) Mank, M.; Griesbeck, O. Genetically Encoded Calcium Indicators. *Chem. Rev.* **2008**, *108*, 1550−1564.

(21) Zou, J.; Hofer, A. M.; Lurtz, M. M.; Gadda, G.; Ellis, A. L.; Chen, N.; Huang, Y.; Holder, A.; Ye, Y.; Louis, C. F.; Welshhans, K.; Rehder, V.; Yang, J. J. Developing Sensors for Real-Time Measurement of High Ca2+ Concentrations. *Biochemistry* **2007**, *46*, 12275−12288.

(22) Presley, K.; Hwang, J.; Cheong, S.; Tilley, R.; Collins, J.; Viapiano, M.; Lannutti, J. Nanoscale upconversion for oxygen sensing. *Mater. Sci. Eng. C* **2017**, *70*, 76−84.

(23) Roussakis, E.; Ortines, R. V.; Pinsker, B. L.; Mooers, C. T.; Evans, C. L.; Miller, L. S.; Calderón-Colón, X. Theranostic biocomposite scaffold membrane. *Biomaterials* **2019**, *212*, 17−27.

(24) Jenkins, J.; Dmitriev, R. I.; Morten, K.; McDermott, K. W.; Papkovsky, D. B. Oxygen-sensing scaffolds for 3-dimensional cell and tissue culture. *Acta Biomater.* **2015**, *16*, 126−135.

(25) O'Donnell, N.; Okkelman, I. A.; Timashev, P.; Gromovykh, T. I.; Papkovsky, D. B.; Dmitriev, R. I. Cellulose-based scaffolds for fluorescence lifetime imaging-assisted tissue engineering. *Acta Biomater.* **2018**, *80*, 85−96.

(26) Yazgan, G.; Dmitriev, R. I.; Tyagi, V.; Jenkins, J.; Rotaru, G.-M.; Rottmar, M.; Rossi, R. M.; Toncelli, C.; Papkovsky, D. B.; Maniura-

Weber, K. Steering surface topographies of electrospun fibers: understanding the mechanisms. *Sci. Rep.* **2017**, *7*, 158.
(27) Giuntini, F.; Chauhan, V. M.; Aylott, J. W.; Rosser, G. A.; Athanasiadis, A.; Beeby, A.; MacRobert, A. J.; Brown, R. A.; Boyle, R. W. Conjugatable water-soluble Pt (II) and Pd (II) porphyrin complexes: novel nano-and molecular probes for optical oxygen tension measurement in tissue engineering. *Photochem. Photobiol. Sci.* **2014**, *13*, 1039−1051.
(28) Boyce, M. W.; Kenney, R. M.; Truong, A. S.; Lockett, M. R. Quantifying oxygen in paper-based cell cultures with luminescent thin film sensors. *Anal. Bioanal. Chem.* **2016**, *408*, 2985−2992.
(29) Rivera, K. R.; Pozdin, V. A.; Young, A. T.; Erb, P. D.; Wisniewski, N. A.; Magness, S. T.; Daniele, M. Integrated phosphorescence-based photonic biosensor (iPOB) for monitoring oxygen levels in 3D cell culture systems. *Biosens. Bioelectron.* **2019**, *123*, 131−140.
(30) Elagin, V.; Kuznetsova, D.; Grebenik, E.; Zolotov, D. A.; Zharikova, T.; Istranova, E.; Polozova, A.; Reunov, D.; Kurkov, A.; Shekhter, A.; Gafarova, E. R.; Asadchikov, V.; Borisov, S. M.; Dmitriev, R. I.; Zagaynova, E.; Timashev, P. Multiparametric Optical Bioimaging Reveals the Fate of Epoxy Crosslinked Biomeshes in the Mouse Subcutaneous Implantation Model. *Front. Bioeng. Biotechnol* **2020**, *8*, 107.
(31) Ishiwari, F.; Hasebe, H.; Matsumura, S.; Hajjaj, F.; Horii-Hayashi, N.; Nishi, M.; Someya, T.; Fukushima, T. Bioinspired design of a polymer gel sensor for the realization of extracellular Ca2+ imaging. *Sci. Rep.* **2016**, *6*, 24275.
(32) Li, Y.; Young, D. J.; Loh, X. J. Fluorescent gels: a review of synthesis, properties, applications and challenges. *Mater. Chem. Front.* **2019**, *3*, 1489−1502.
(33) Gao, M.; Li, Y.; Chen, X.; Li, S.; Ren, L.; Tang, B. Z. Aggregation-Induced Emission Probe for Light-Up and in Situ Detection of Calcium Ions at High Concentration. *ACS Appl. Mater. Interfaces* **2018**, *10*, 14410−14417.
(34) Babilas, P.; Liebsch, G.; Schacht, V.; Klimant, I.; Wolfbeis, O. S.; Szeimies, R.-M.; Abels, C. In vivo phosphorescence imaging of pO2 using planar oxygen sensors. *Microcirculation* **2005**, *12*, 477−487.
(35) Papkovsky, D. B.; Dmitriev, R. I. Biological detection by optical oxygen sensing. *Chem. Soc. Rev.* **2013**, *42*, 8700−8732.
(36) Roussakis, E.; Li, Z.; Nichols, A. J.; Evans, C. L. Oxygen-sensing methods in biomedicine from the macroscale to the microscale. *Angew. Chem., Int. Ed.* **2015**, *54*, 8340−8362.
(37) Schreml, S.; Meier, R. J.; Wolfbeis, O. S.; Maisch, T.; Szeimies, R.-M.; Landthaler, M.; Regensburger, J.; Santarelli, F.; Klimant, I.; Babilas, P. 2D luminescence imaging of physiological wound oxygenation. *Exp. Dermatol.* **2011**, *20*, 550−554.
(38) Consolati, T.; Bolivar, J. M.; Petrasek, Z.; Berenguer, J.; Hidalgo, A.; Guisán, J. M.; Nidetzky, B. Bio-based, internally pH sensitive materials: immobilized yellow fluorescent protein as optical sensor for spatiotemporal mapping of pH inside porous matrices. *ACS Appl. Mater. Interfaces* **2018**, *10*, 6858−6868.
(39) Schyrr, B.; Pasche, S.; Voirin, G.; Weder, C.; Simon, Y. C.; Foster, E. J. Biosensors Based on Porous Cellulose Nanocrystal−Poly(vinyl Alcohol) Scaffolds. *ACS Appl. Mater. Interfaces* **2014**, *6*, 12674−12683.
(40) Nakai, J.; Ohkura, M.; Imoto, K. A high signal-to-noise Ca2+ probe composed of a single green fluorescent protein. *Nat. Biotechnol.* **2001**, *19*, 137−141.
(41) Gensch, T.; Kaschuba, D. Fluorescent genetically encoded calcium indicators and their in vivo application. *Fluorescent Proteins II*; Springer, 2011; pp 125−161.
(42) Díaz-García, C. M.; Mongeon, R.; Lahmann, C.; Koveal, D.; Zucker, H.; Yellen, G. Neuronal stimulation triggers neuronal glycolysis and not lactate uptake. *Cell Metab.* **2017**, *26*, 361−374.
(43) Rinnenthal, J. L.; Börnchen, C.; Radbruch, H.; Andresen, V.; Mossakowski, A.; Siffrin, V.; Seelemann, T.; Spiecker, H.; Moll, I.; Herz, J. Parallelized TCSPC for dynamic intravital fluorescence lifetime imaging: quantifying neuronal dysfunction in neuroinflammation. *PLoS One* **2013**, *8*, No. e60100.
(44) Thestrup, T.; Litzlbauer, J.; Bartholomäus, I.; Mues, M.; Russo, L.; Dana, H.; Kovalchuk, Y.; Liang, Y.; Kalamakis, G.; Laukat, Y.; Becker, S.; Witte, G.; Geiger, A.; Allen, T.; Rome, L. C.; Chen, T.-W.; Kim, D. S.; Garaschuk, O.; Griesinger, C.; Griesbeck, O. Optimized ratiometric calcium sensors for functional in vivo imaging of neurons and T lymphocytes. *Nat. Methods* **2014**, *11*, 175.
(45) Rakymzhan, A.; Radbruch, H.; Niesner, R. A. Quantitative Imaging of Ca 2+ by 3D−FLIM in Live Tissues. *Multi-Parametric Live Cell Microscopy of 3D Tissue Models*; Springer, 2017; pp 135−141.
(46) Suhling, K.; Hirvonen, L. M.; Levitt, J. A.; Chung, P.-H.; Tregidgo, C.; Le Marois, A.; Rusakov, D. A.; Zheng, K.; Ameer-Beg, S.; Poland, S. Fluorescence lifetime imaging (FLIM): Basic concepts and some recent developments. *Med. Photon.* **2015**, *27*, 3−40.
(47) Dmitriev, R. I.; Kondrashina, A. V.; Koren, K.; Klimant, I.; Zhdanov, A. V.; Pakan, J. M. P.; McDermott, K. W.; Papkovsky, D. B. Small molecule phosphorescent probes for O 2 imaging in 3D tissue models. *Biomater. Sci.* **2014**, *2*, 853−866.
(48) Zhdanov, A. V.; Dmitriev, R. I.; Hynes, J.; Papkovsky, D. B. Kinetic analysis of local oxygenation and respiratory responses of Mammalian cells using intracellular oxygen-sensitive probes and time-resolved fluorometry. *Methods Enzymol.* **2014**, *542*, 183−207.
(49) Okkelman, I. A.; Neto, N.; Papkovsky, D. B.; Monaghan, M. G.; Dmitriev, R. I. A deeper understanding of intestinal organoid metabolism revealed by combining fluorescence lifetime imaging microscopy (FLIM) and extracellular flux analyses. *Redox Biol.* **2020**, *30*, 101420.
(50) Okkelman, I. A.; Papkovsky, D. B.; Dmitriev, R. I. Estimation of the Mitochondrial Membrane Potential Using Fluorescence Lifetime Imaging Microscopy. *Cytometry, Part A* **2019**, *97*, 471−482.
(51) Okkelman, I. A.; Puschhof, J.; Papkovsky, D. B.; Dmitriev, R. I. Visualization of Stem Cell Niche by Fluorescence Lifetime Imaging Microscopy. In *Intestinal Stem Cells: Methods and Protocols*; Ordonez-Moran, P., Ed.; Springer Science + Business Media, LLC, Part of Springer Nature 2020: Springer US, 2020; Vol. *2171*.
(52) Takagi, J.; Asai, H.; Saito, Y. A collagen/gelatin-binding decapeptide derived from bovine propolypeptide of von Willebrand factor. *Biochemistry* **1992**, *31*, 8530−8534.
(53) Evanko, D. S.; Haydon, P. G. Elimination of environmental sensitivity in a cameleon FRET-based calcium sensor via replacement of the acceptor with Venus. *Cell Calcium* **2005**, *37*, 341−348.
(54) Sato, T.; Vries, R. G.; Snippert, H. J.; van de Wetering, M.; Barker, N.; Stange, D. E.; van Es, J. H.; Abo, A.; Peters, P. J.; Clevers, H. Single Lgr5 stem cells build crypt−villus structures in vitro without a mesenchymal niche. *Nature* **2009**, *459*, 262.
(55) Gjorevski, N.; Sachs, N.; Manfrin, A.; Giger, S.; Bragina, M. E.; Ordóñez-Morán, P.; Clevers, H.; Lutolf, M. P. Designer matrices for intestinal stem cell and organoid culture. *Nature* **2016**, *539*, 560.
(56) Okkelman, I. A.; Dmitriev, R. I.; Foley, T.; Papkovsky, D. B. Use of Fluorescence Lifetime Imaging Microscopy (FLIM) as a Timer of Cell Cycle S Phase. *PLoS One* **2016**, *11*, No. e0167385.
(57) Okkelman, I. A.; Foley, T.; Papkovsky, D. B.; Dmitriev, R. I. Live cell imaging of mouse intestinal organoids reveals heterogeneity in their oxygenation. *Biomaterials* **2017**, *146*, 86−96.
(58) Levitt, J. A.; Chung, P.-H.; Suhling, K. Spectrally resolved fluorescence lifetime imaging of Nile red for measurements of intracellular polarity. *J. Biomed. Opt.* **2015**, *20*, 096002.
(59) Papahadjopoulos, D.; Vail, W. J.; Pangborn, W. A.; Poste, G. Studies on membrane fusion. II. Induction of fusion in pure phospholipid membranes by calcium ions and other divalent metals. *Biochim. Biophys. Acta Biomembr.* **1976**, *448*, 265−283.
(60) Bush, K. T.; Lee, H.; Nagele, R. G. Lipid droplets of neuroepithelial cells are a major calcium storage site during neural tube formation in chick and mouse embryos. *Experientia* **1992**, *48*, 516−519.
(61) Barba, I.; Chavarria, L.; Ruiz-Meana, M.; Mirabet, M.; Agulló, E.; Garcia-Dorado, D. Effect of intracellular lipid droplets on cytosolic Ca2+ and cell death during ischaemia−reperfusion injury in cardiomyocytes. *J. Physiol.* **2009**, *587*, 1331−1341.

https://dx.doi.org/10.1021/acsabm.0c00649
ACS Appl. Bio Mater. 2020, 3, 5310−5321

(62) Silvagno, F.; Pescarmona, G. Spotlight on vitamin D receptor, lipid metabolism and mitochondria: Some preliminary emerging issues. *Mol. Cell. Endocrinol.* **2017**, *450*, 24−31.
(63) Tsai, H. C.; Wong, R. G.; Norman, A. W. Studies on calciferol metabolism: iv. Subcellular localization of 1,25-dihydroxy-vitamin d3 in intestinal mucosa and correlation with increased calcium transport. *J. Biol. Chem.* **1972**, *247*, 5511−5519.
(64) Diaz, G.; Melis, M.; Batetta, B.; Angius, F.; Falchi, A. M. Hydrophobic characterization of intracellular lipids in situ by Nile Red red/yellow emission ratio. *Micron* **2008**, *39*, 819−824.
(65) Giudici, C.; Raynal, N.; Wiedemann, H.; Cabral, W. A.; Marini, J. C.; Timpl, R.; Bächinger, H. P.; Farndale, R. W.; Sasaki, T.; Tenni, R. Mapping of SPARC/BM-40/Osteonectin-binding Sites on Fibrillar Collagens. *J. Biol. Chem.* **2008**, *283*, 19551−19560.
(66) Mayer, U.; Aumailley, M.; Mann, K.; Timpl, R.; Engel, J. Calcium-dependent binding of basement membrane protein BM-40 (osteonectin, SPARC) to basement membrane collagen type IV. *Eur. J. Biochem.* **1991**, *198*, 141−150.
(67) Greineisen, W. E.; Speck, M.; Shimoda, L. M. N.; Sung, C.; Phan, N.; Maaetoft-Udsen, K.; Stokes, A. J.; Turner, H. Lipid body accumulation alters calcium signaling dynamics in immune cells. *Cell Calcium* **2014**, *56*, 169−180.
(68) Lattarulo, C.; Thyssen, D.; Kuchibholta, K. V.; Hyman, B. T.; Bacskaiq, B. J. Microscopic imaging of intracellular calcium in live cells using lifetime-based ratiometric measurements of Oregon Green BAPTA-1. *Neurodegeneration*; Springer, 2011; pp 377−389.

https://dx.doi.org/10.1021/acsabm.0c00649
ACS Appl. Bio Mater. 2020, 3, 5310−5321